Title
Effect of Alcohol Structure on the Kinetics of Etherification and Dehydration over Tungstated Zirconia

Journal
ChemSusChem, 11(18)

ISSN
1864-5631

Authors
Rorrer, Julie
Pindi, Suresh
Toste, F Dean
et al.

Publication Date
2018-09-21

DOI
10.1002/cssc.201801067

Peer reviewed

ChemPubSoc Europe

DOI: 10.1002/cssc.201801067

CHEMSUSCHEM Full Papers

Effect of Alcohol Structure on the Kinetics of Etherification and Dehydration over Tungstated Zirconia

Julie Rorrer,[a, b] Suresh Pindi,[a, c] F. Dean Toste,[a, c] and Alexis T. Bell*[a, b]

Linear and branched ether molecules have attracted recent interest as diesel additives and lubricants that can be produced from biomass-derived alcohols. In this study, tungstated zirconia was identified as a selective and green solid acid catalyst for the direct etherification of primary alcohols in the liquid phase, achieving ether selectivities of >94% for C_6–C_{12} linear alcohol coupling at 393 K. The length of linear primary alcohols (C_6–C_{12}) was shown to have a negligible effect on apparent activation energies for etherification and dehydration, demonstrating the possibility to produce both symmetrical and asymmetrical linear ethers. Reactions over a series of C_6 alcohols with varying methyl branch positions indicated that substituted alcohols (2°, 3°) and alcohols with branches on the β-carbon readily undergo dehydration, but alcohols with branches at least three carbons away from the -OH group are highly selective to ether. A novel model compound, 4-hexyl-1-dodecanol, was synthesized and tested to further demonstrate this structure–activity relationship. Trends in the effects of alcohol structure on selectivity were consistent with previously proposed mechanisms for etherification and dehydration, and help to define possible pathways to selectively form ethers from biomass-derived alcohols.

Introduction

As the adverse effects of anthropogenic climate change continue to increase, the global need for clean and renewable energy is now larger than ever before. One method of lowering net atmospheric CO_2 emissions is to replace conventional fossil fuels and petroleum-derived specialty chemicals with renewable alternatives.[1] Ethers have attracted recent interest as renewable fuels and lubricants. Symmetric and asymmetric linear ethers in the C_8–C_{12} range are suitable diesel additives owing to their high cetane numbers.[2–5] Branched ethers such as methyl *tert*-butyl ether can also be added to gasoline because of their high octane numbers.[6] Longer chain branched ethers in the C_{28}–C_{32} range have low pour points and excellent lubricant properties,[7–9] and could replace poly-alpha-olefin lubricants, which are produced from fossil reserves.[10,11]

Biomass-derived alcohols are promising candidates for producing renewable ethers. Ethanol and butanol can be obtained in high yields through fermentation processes such as ABE (acetone–butanol–ethanol) fermentation.[12–14] Longer chain linear alcohols such as 1-octanol and 1-dodecanol can be produced from the condensation of biomass-derived furan platform molecules, and the hydrolysis of triglycerides and fatty acids, respectively,[15] and then built up into branched alcohols with higher carbon numbers through the Guerbet reaction.[16] Some general approaches to producing linear and branched alcohols from biomass-derived platform molecules are summarized in Scheme 1.

Direct etherification of biomass-derived alcohols over an acid catalyst is an attractive method of producing ethers because it does not require hydrogen gas and precious metal catalysts like reductive etherification.[17] The competing reaction for alcohol dehydration over an acid catalyst is unimolecular dehydration to form alkenes, which is thermodynamically favored at temperatures above approximately 350 K. Owing to their high volatility, and the propensity to form gums, alkenes are not desired in fuel and lubricant blends.[18]

In a previous study, tungstated zirconia was identified as a selective catalyst for the liquid-phase etherification of 1-dodecanol, with ether selectivities above 94% at moderate temperatures (393 K).[19] This study suggested that the high selectivity to ether is due to a cooperative effect between Brønsted- and Lewis-acid sites on the surface of the catalyst, which promotes the bi-molecular etherification reaction. This research motivates the current study, which aims to evaluate the extent to which tungstated zirconia can be used to produce a variety of symmetrical and asymmetrical ethers, and mixtures of ethers, for fuel and lubricant applications.

Kinetic studies of alcohol dehydration reactions have traditionally been centered on gas-phase unimolecular dehydration.[20–22] Experimental and computational studies of gas-

[a] J. Rorrer, Dr. S. Pindi, Prof. F. D. Toste, Prof. A. T. Bell
Energy Biosciences Institute
University of California
Berkeley, CA 94720 (USA)
E-mail: alexbell@berkeley.edu

[b] J. Rorrer, Prof. A. T. Bell
Department of Chemical and Biomolecular Engineering
University of California
Berkeley, CA 94720 (USA)

[c] Dr. S. Pindi, Prof. F. D. Toste
Department of Chemistry
University of California
Berkeley, CA 94720 (USA)

Supporting Information and the ORCID identification number(s) for the author(s) of this article can be found under: https://doi.org/10.1002/cssc.201801067.

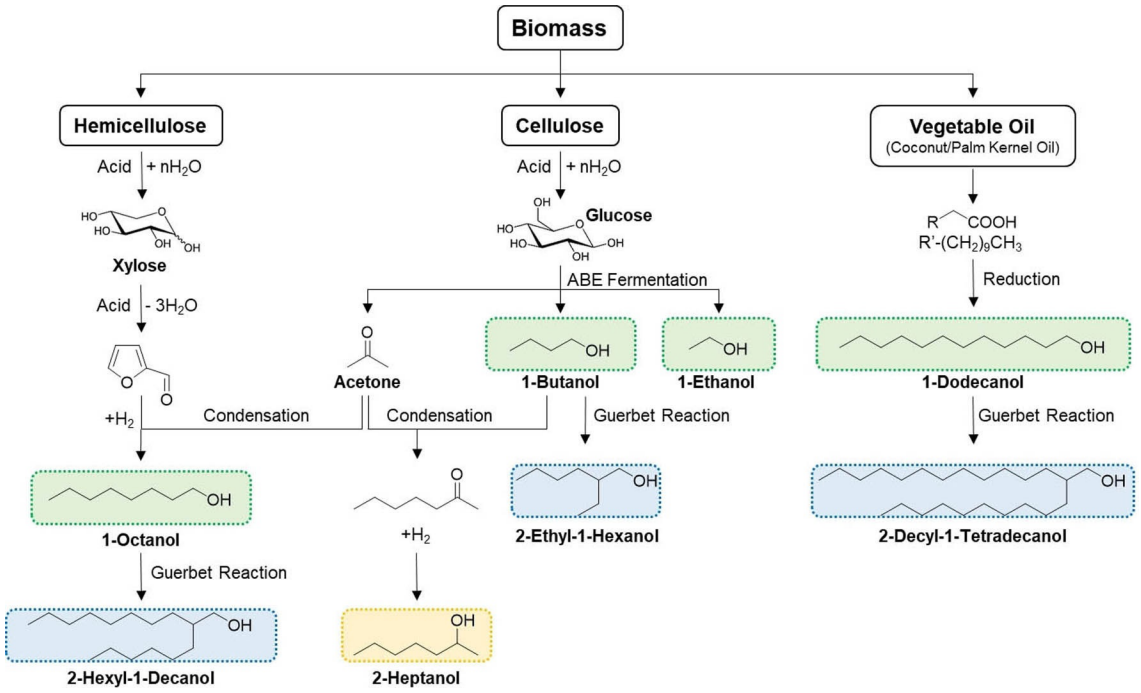

Scheme 1. General approach to producing linear and branched alcohols from biomass-derived platform molecules.

phase unimolecular dehydration of alcohols over γ-Al_2O_3 have supported the theory that increasing the substitution of the alcohol increases the stability of the intermediate in the rate-limiting step for dehydration, resulting in a decrease in activation barrier for dehydration with increasing substitution.[20,23]

Although studying the effect of alcohol structure in the gas phase where unimolecular dehydration dominates has provided some insight into the relationship between unimolecular dehydration rates and substitution, the kinetics of etherification must also be explored to understand the relationship between alcohol structure and selectivity to ether. Some efforts have been made to investigate the catalytic conversion of alcohols to both symmetrical and asymmetrical ethers at moderate temperatures where etherification dominates. Various acidic resins and zeolites have been shown to be effective in the liquid-phase etherification of 1-pentanol, 1-hexanol, and 1-octanol to produce symmetrical ethers.[24–27] Tejero et al. have demonstrated that it is also possible to produce asymmetrical ethers like ethyl-hexyl ether and ethyl-octyl ether through cross-coupling of 1-hexanol or 1-octanol with ethanol or diethylcarbonate.[5,28]

But, to our knowledge, the literature is lacking a comprehensive study of the kinetics of liquid-phase etherification reactions over a large range of long-chain 1-alcohols (C_6–C_{12}), and a more thorough investigation into the effect of branched alcohols on the formation of symmetrical and asymmetrical ethers in the lubricant range (C_{12}–C_{36}). Although acidic resins such as Amberlyst 70 and Nafion NR-50 have been shown to be effective for etherification of linear alcohols in the liquid phase, measuring accurate rate data is difficult owing to the swelling of these resins in the solvent, which causes changes in the number of accessible active sites over time.[29] Tungstated zirconia is thermally stable, does not deactivate or swell in the reactant media, and has been shown to be an effective catalyst for etherification of alcohols. Thus, this paper will comprehensively study the effects of linear alcohol length, carbon chain branches, and positions of carbon chain branches on the kinetics of etherification and dehydration reactions over tungstated zirconia in the liquid phase, with the aim of understanding the relationship between ether selectivity and alcohol structure.

Results and Discussion

Catalyst characterization

Tungstated zirconia (WO_x/ZrO_2, 12.6 wt% W) was characterized with X-ray diffraction, Raman spectroscopy, and diffuse reflectance infrared Fourier transform spectroscopy (DRIFTS) FTIR with adsorbed pyridine to determine the structure and confirm the presence of Brønsted- and Lewis-acid sites. From the XRD pattern in Figure 1a, the peaks at 2θ angles of 30, 35, 50, and 59° (yellow) indicate the presence of tetragonal zirconia,[30–32] and the peaks between 23–25° (pink) represent the presence of bulk tungsten oxide.[33] From the Raman spectra in Figure 1b, the bands at 274, 715, and 807 cm^{-1} (pink) indicate the W–O stretching of bulk tungsten oxide,[34] and the band at 1020 cm^{-1} (yellow) is indicative of polymeric tungsten oxide terminated by a tungsten oxygen double bond.[35] The DRIFTS FTIR spectra of adsorbed pyridine shown in Figure 1c demonstrates that both Brønsted- and Lewis-acid sites are present on the surface of the catalyst, as evident from bands of adsorbed pyridine at 1540 cm^{-1} (blue) and 1444 cm^{-1} (green), respectively. Additional catalyst characterization is summarized in Table 1.

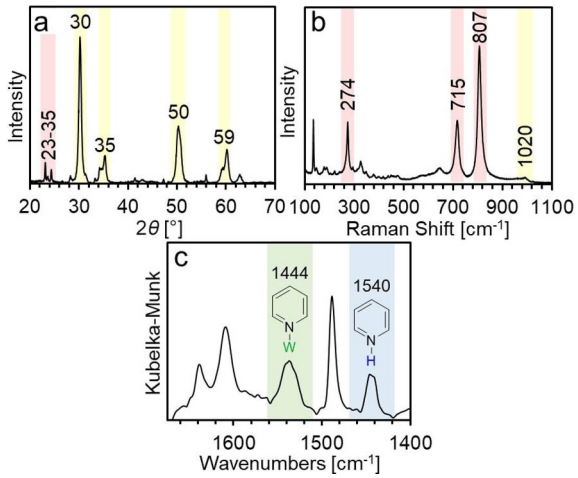

Figure 1. Characterization of 12.6 wt% W (WO_x/ZrO_2): a) X-ray diffraction pattern, b) Raman spectrum, c) DRIFTS FTIR spectrum of adsorbed pyridine at 393 K.

Table 1. Characterization of 12.6 wt% WO_x/ZrO_2.

Property	Value
weight loading of W [%]	12.6
zirconia crystal structure (XRD)	tetragonal
BET surface area [$m^2 g^{-1}$]	51
Brønsted acid sites [mol eq. H^+ m^{-2}]	$1.78\times10^{-6}\pm1.4\times10^{-7}$
ratio of Brønsted/Lewis acid sites	0.90 ± 0.02 (393 K)

Effect of alcohol structure on kinetics: linear primary alcohols (C_6–C_{12})

To build symmetrical and asymmetrical linear ethers in the diesel range, it is necessary to investigate the effect of alcohol chain length on the apparent kinetics of etherification and dehydration over tungstated zirconia. The selectivity to ether for C_6–C_{12} alcohols (1-hexanol, 1-heptanol, 1-octanol, 1-nonanol, 1-decanol, 1-undecanol, and 1-dodecanol) was measured for temperatures between 393–418 K. The results are summarized in Table 2.

Table 2. Selectivity of primary linear alcohols (C_6–C_{12}) to symmetrical ethers (C_{12}–C_{24}) over tungstated zirconia with varying temperature.[a]

Reactant	Selectivity to symmetrical ether [%]/(Conversion of alcohol [%])					
	393 K	398 K	403 K	408 K	413 K	418 K
1-hexanol	>99/(4)	94/(6)	88/(11)	88/(22)	89/(27)	87/(39)
1-heptanol	>99/(5)	80/(7)	80/(11)	82/(26)	80/(25)	80/(38)
1-octanol	>99/(4)	92/(6)	92/(12)	83/(20)	85/(28)	80/(33)
1-nonanol	>99/(4)	89/(7)	85/(12)	86/(20)	81/(28)	77/(37)
1-decanol	>99/(4)	95/(8)	94/(11)	90/(18)	88/(25)	85/(38)
1-undecanol	>99/(5)	92/(6)	89/(9)	88/(17)	82/(25)	78/(42)
1-dodecanol	94/(6)	94/(7)	86/(11)	83/(26)	80/(30)	84/(38)

[a] Reaction Conditions: 1 h, 100 mg WO_x/ZrO_2 (12.6 wt% W), 600 RPM, 564 μmol reactant, 125 μmol *n*-tetradecane. Remaining selectivity is attributed to alkenes and trace amounts of branched ether. Error within ±2% for data at 393–413 K, and within ±4% for 418 K.

For all of the linear alcohols studied, the selectivity to ether decreases with increasing temperature. However, the carbon chain length does not appear to have any significant effect on the selectivity. Nel and De Klerk observed that ether selectivity of C_6–C_{12} linear alcohols decreased with increasing carbon chain length for gas-phase reactions over η-alumina at 523 K.[2] The authors claimed that their system was limited by external mass transfer, which could explain why they observed a decrease in selectivity for longer chain alcohols.

The apparent activation energies for etherification and dehydration of linear alcohols in the liquid phase were obtained by measuring the initial rates of ether and alkene formation over a range of temperatures. A sample time-course study of 1-dodecanol etherification over WO_x/ZrO_2 (12.6 wt% W) at 393 K is shown in Figure S1 in the Supporting Information, which demonstrates that at conversions below approximately 25%, the kinetics are pseudo-zeroth order. The rates, selectivities, Arrhenius plots, and temperature ranges for which the initial rates were obtained are provided in Figure S2 and Tables S1–S2 in the Supporting Information.

Figure 2 shows the apparent activation energies for etherification and dehydration of primary linear alcohols 1-hexanol, 1-heptanol, 1-octanol, 1-nonanol, 1-decanol, 1-undecanol, and 1-dodecanol. Overall, the activation barriers for unimolecular dehydration in Figure 2b (154–157 kJ mol^{-1}) are greater than the activation barriers for etherification in Figure 2a (126–127 kJ mol^{-1}), which explains the decrease in selectivity to ether with increasing temperature observed in Table 2. The activation energies for linear alcohol etherification do not change significantly with increasing carbon chain length, implying that the length of linear alcohols has little effect on the kinetics of etherification and dehydration.

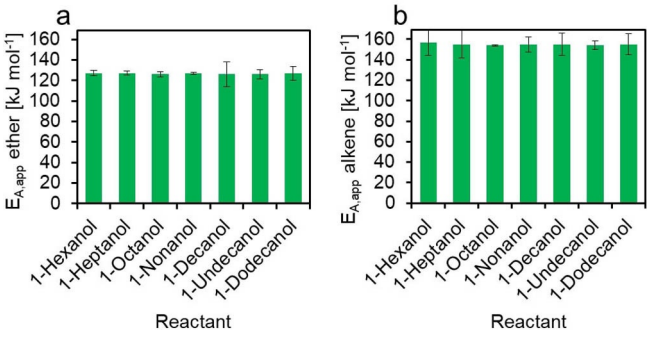

Figure 2. a) Apparent activation energies for etherification, b) apparent activation energies for dehydration of C_6–C_{12} primary alcohols over WO_x/ZrO_2 (12.6 wt% W).

For applications in diesel fuel, mixtures of linear alcohols could be tuned in the reactant feed to create a distribution of ethers that contains a desired molecular weight distribution. A similar tuning of molecular weights has been demonstrated previously for the trimerization of ketones for diesel fuel mixtures.[36] Because the etherification activation ener-

gies and reaction rates do not vary significantly between linear alcohols in the C_6–C_{12} range, a mixture of alcohols will couple in a nearly random statistical distribution. An example distribution study is shown in Figure 3. Seven linear alcohols (1-hexanol, 1-heptanol, 1-octanol, 1-nonanol, 1-decanol, 1-undecanol, and 1-dodecanol) in equimolar ratios were reacted together over tungstated zirconia at 393 K. The theoretical selectivity distribution for random cross-coupling of alcohols is shown in black, and the experimental distribution of ether products is shown in green. Figure 3 shows that there is a slight preference for coupling of the shorter chain alcohols, which could be explained by the fact that the experiment was run at high conversion (>90%), where the inhibiting effects of water and ether are no longer negligible. Under these conditions, it is possible that the bulkier ethers such as di-dodecyl ether introduce steric effects and thus have a greater inhibiting effect on the rate of consumption of the longer chain alcohols. The observation that cross-coupling of linear alcohols is nearly statistical suggests that the distribution of linear alcohols in the feed could be tuned to produce a variety of desired ether blends.

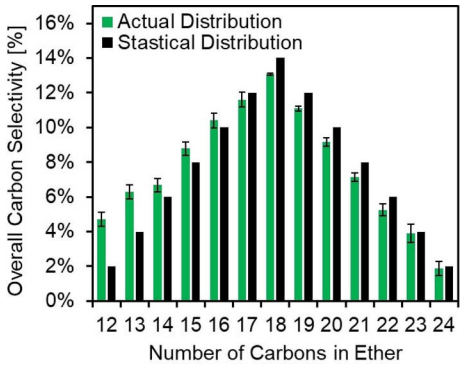

Figure 3. Ether distribution for C_6–C_{12} alcohols. Reaction conditions: 393 K, 48 h, 100 mg WO_x/ZrO_2 (12.6 wt% W), 600 RPM. Equimolar ratio of 1-hexanol, 1-heptanol, 1-octanol, 1-nonanol, 1-decanol, 1-undecanol, and 1-dodecanol, with *n*-tetradecane as an internal standard. Conversion >90%.

Effect of alcohol structure on kinetics: position of carbon chain branches

To systematically study the effect of the position of carbon chain branches on etherification kinetics, a series of C_6 alcohols with varying degrees of substitution and positions of methyl groups were reacted over tungstated zirconia. Table 3 shows the selectivity to ether for the C_6 alcohols at 393 K. Primary C_6 alcohols with a methyl group at least three carbons away from the -OH group (1-hexanol, 4-methyl-1-pentanol, and 3-methyl-1-pentanol) exhibit a very high selectivity to ether. As the methyl group approaches the β-carbon (2-methyl-1-pentanol), the ether selectivity rapidly decreases. Secondary and tertiary C_6 alcohols (2-hexanol and 2-methyl-2-pentanol) rapidly dehydrated under these conditions, forming no ether.

To further study the relationship between branching position and kinetics, the apparent activation energies of etherification and dehydration of the C_6 alcohols were measured, and are shown in Figure 4. Temperature ranges were selected such that initial rates of both ether and alkene could be measured, with the exception of 2-methyl-2-pentanol, for which ether could not be detected at any of the temperatures in the range of 333–418 K. The initial rates, Arrhenius plots, and temperature ranges are provided in Figure S3 and Tables S3–S4 in the Supporting Information.

Table 3. Selectivity of reactions over C_6 alcohols.[a]

Reactant	Conv. [%]	Sel. [%] ether	alkenes/other
1-hexanol	11	>99	<1
4-methyl-1-pentanol	10	>99	<1
3-methyl-1-pentanol	10	87	13
2-methyl-1-pentanol	14	<1	>99
2-hexanol	>99	<1	>99
2-methyl-2-pentanol	>99	<1	>99

[a] Reaction conditions: 393 K, 4 h, 100 mg WO_x/ZrO_2 (12.6 wt% W), 600 RPM, 168 μL reactant, 100 μL *n*-tetradecane as internal standard.

Figure 4a shows that the apparent activation barrier for etherification is fairly independent of the reactant. But from Figure 4b, it is clear that as the substitution of the alcohol increases, the barrier for unimolecular dehydration decreases. The dehydration activation barriers for 1-hexanol, 4-methyl-1-pentanol, and 3-methyl-1-pentanol are 157±13, 158±10, and 155±1 kJ mol^{-1}, respectively, indicating that the barriers are within error for alcohols with branching at least three carbons away from the -OH group. But for 2-methyl-1-pentanol, 2-hexanol, and 2-methyl-2-pentanol, the barriers are 124±2, 114±5, and 100±12 kJ mol^{-1}, respectively, indicating that the dehydration barrier decreases with increasing substitution of the alcohol. In our previous study, measurements of kinetic isotope effects for 1-hexanol dehydration over tungstated zirconia suggested that the rate-limiting step for unimolecular dehydration is the cleavage of a β-carbon hydrogen bond.[19] This is consistent with the findings in Figure 4, as the increased sub-

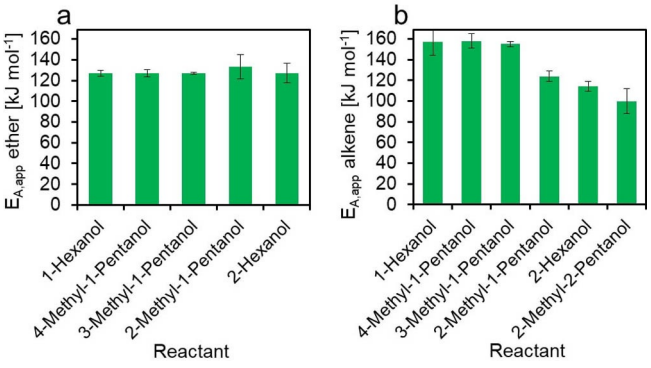

Figure 4. a) Apparent activation energies for etherification, b) apparent activation energies for dehydration of C_6 alcohols (1-hexanol, 4-methyl-1-pentanol, 3-methyl-1-pentanol, 2-methyl-1-pentanol, 2-hexanol, and 2-methyl-2-pentanol) over WO_x/ZrO_2 (12.6 wt% W).

stitution of the α- and β-carbons would increase the stability of the carbocation intermediate formed during unimolecular dehydration, making dehydration more favorable. Also found in our previous study, the dehydration of 1-hexanol produced both 1-hexene and 2-hexene, as verified by NMR spectroscopy; however, no methyl shift was observed, as might be expected for the dehydration of a substrate such as 3,3-di-methyl-2-butanol.[19,37]

In addition, steric effects that limit α-carbon oxygen bond formation between two alcohols could explain the preference towards unimolecular dehydration for 2° and 3° alcohols.[23] Similar relationships between alcohol structure and dehydration activation barriers have been observed in the literature for other solid acid catalysts. Activation energies of 145, 141, 121, and 110 kJ mol^{-1} have been reported for gas-phase unimolecular dehydration of ethanol, 1-propanol, 2-propanol, and 2-methyl-2-propanol, respectively, over γ-Al_2O_3, indicating that increasing substitution decreases the activation barrier for unimolecular dehydration.[20,23] Mpourmpakis et al. observed that dehydration activation barriers of ethanol, 1-propanol, 2-propanol, and 2-methyl-2-propanol also decreased with increasing substitution for dehydration reactions over γ-Al_2O_3, ZrO_2, and TiO_2.[21] The relationship between alcohol substitution and reactivity for unimolecular dehydration is in agreement with the results presented here for C_6 alcohols in the liquid phase, and the relative activation energies for etherification provide an explanation for the selectivity trends observed in Table 3.

Effect of alcohol structure: length of carbon chain branches

Although the kinetics of linear alcohols do not vary significantly from C_6–C_{12}, the addition of branches changes the selectivity to ether. To further investigate the effects of branch size on ether selectivity, a series of Guerbet alcohols with increasing carbon chain backbone length and branch length were reacted with 1-dodecanol in 1:1 molar ratios at low conversions to form symmetrical and asymmetrical ethers in the lubricant range (C_{16}–C_{36}). The pathways for these reactions are shown in Scheme 2, and the results are summarized in Table 4. Symmetrical branched ethers (1E) are only formed in small amounts from the coupling of small Guerbet alcohols (2-ethyl-1-hexanol and 2-butyl-1-octanol), and are not formed from the coupling of bulkier alcohols ($>C_{16}$). In addition, the reactivity of Guerbet alcohols decreases with increasing bulkiness.

The relatively low selectivity towards branched ethers from the etherification of Guerbet alcohols is likely due to the relatively low activation barrier for unimolecular dehydration of alcohols with substitution on the β-carbon. From Table 3, the addition of methyl branches affected the selectivity to ether to a lesser extent when the branch was three carbons away from the -OH group. Thus, it was hypothesized that etherification of a longer chain branched alcohol with the branch further down the carbon chain would result in higher selectivity to ether than a Guerbet alcohol of the same chain length. To test this, the model compound 4-hexyl-1-dodecanol was synthesized and reacted over tungstated zirconia at 393 K, as shown in Scheme 3. The synthesis and characterization of 4-hexyl-1-dodecanol is detailed in the Supporting Information.

From Table 5, it can be observed that there is significant improvement in selectivity to ether for the C_{18} alcohol when the branching position is further away from the -OH group, reaching 40% selectivity to ether (2B) at a conversion of 23% at 393 K. Upon lowering the temperature to 383 K, the selectivity was further increased to 49%, which is expected as etherification was shown to be more favorable at lower temperatures. The results given in Table 4 indicate that 2-hexyl-1-decanol (C_{16}) and 2-octyl-1-dodecanol (C_{20}) do not produce symmetrical ethers in reactions with 1-dodecanol over tungstated zirconia. For additional comparison, Guerbet alcohols 2-hexyl-1-decanol and 2-octyl-1-dodecanol were also reacted over tungstated zirconia under the same conditions as those used for the reaction of 4-hexyl-1-dodecanol in the absence of 1-dodecanol. No ether was detected for either of these reactions (Table S6 in the Supporting Information).

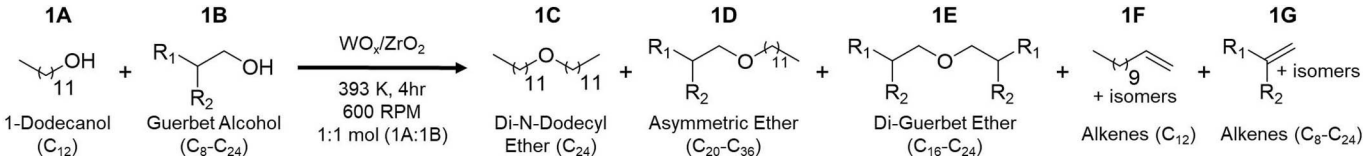

Scheme 2. Pathways for 1-dodecanol etherification and dehydration with varying Guerbet alcohols (C_8–C_{24}) over tungstated zirconia.

Table 4. Effect of branch length of Guerbet alcohols on the selectivity of ethers and alkenes in reaction with 1-dodecanol.[a]

Guerbet alcohol	R_1	R_2	Conv. 1A [%]	Dodecanol sel. [%] 1C	1D	1F	Conv. 1B [%]	Guerbet alcohol sel. [%] 1D	1E	1G
2-ethyl-1-hexanol	4	2	14	63	20	16	33	11	3	86
2-butyl-1-octanol	6	4	18	69	16	15	26	11	1	89
2-hexyl-1-decanol	8	6	21	71	10	20	13	18	0	82
2-octyl-1-dodecanol	10	8	23	72	7	21	9	20	0	80
2-decyl-1-tetradecanol	12	10	23	72	6	22	3	17	0	83

[a] Reaction conditions: 393 K, 4 h, 100 mg WO_x/ZrO_2 (12.6 wt% W), 600 RPM, 5.6×10^{-4} mol 1-dodecanol, 5.6×10^{-4} mol Guerbet alcohol, 3.9×10^{-4} mol *n*-tetradecane as internal standard.

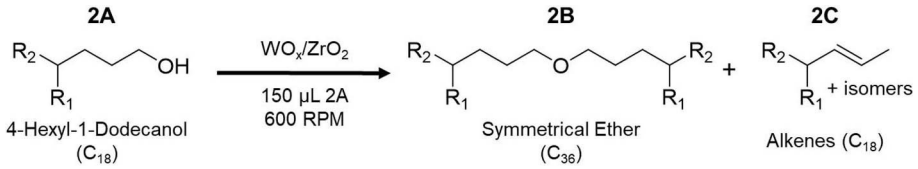

Scheme 3. Reaction of 4-hexyl-1-dodecanol over tungstated zirconia.

Table 5. Etherification and dehydration of 4-hexyl-1-dodecanol.[a]

Alcohol	R_1	R_2	T [K]	Reaction time [h]	Conv. alcohol [%]	Sel. [%] ether	alkenes
4-hexyl-1-dodecanol	6	8	393	4	23	40	60
4-hexyl-1-dodecanol	6	8	383	4	11	49	51
4-hexyl-1-dodecanol	6	8	383	16	22	52	48

[a] Reaction conditions: 100 mg WO_x/ZrO_2 (12.6 wt% W), 600 RPM, 150 µL 4-hexyl-1-dodecanol, 3.9×10^{-4} mol *n*-tetradecane as internal standard. Note: 10% mass balance missing for 16 h reaction.

Thus, placing the branch further away from the -OH group of the alcohol significantly improves the selectivity to ether. This raises the question of how branched alcohols with branches further down the carbon chain could be produced from biomass. One potential route would be to start with the condensation of biomass-derived furfural and 2-methylfuran,[38] then selectively hydrogenate to produce 5-pentyl-1-decanol, which could further be reacted over an acid catalyst to form ether, as shown in Scheme 4.

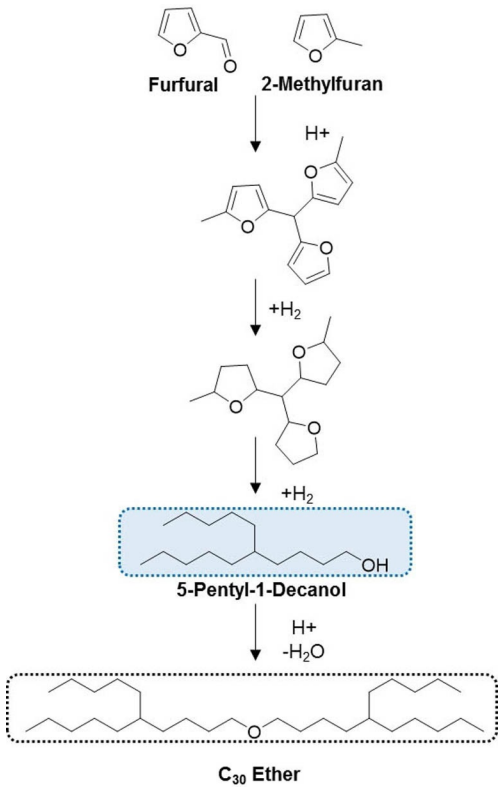

Scheme 4. Proposed route to produce branched lubricants from biomass-derived platform molecules.

Conclusions

Tungstated zirconia was identified as an effective solid acid catalyst for the direct etherification of primary linear alcohols in the liquid phase. The effect of alcohol structure on etherification and dehydration reactions was studied by investigating the effects of alcohol length, positions of carbon chain branches, and size of carbon chain branches. The rate of dehydration relative to etherification was shown to increase with increasing temperature, which is consistent with the thermodynamic preference for dehydration with increasing temperature. The positions of carbon chain branches were shown to have significant effects on ether selectivity. Addition of carbon chain branches to the α- and β-carbons on the alcohol were shown to increase the dehydration selectivity, which is consistent with the mechanism proposed in an earlier work. It was also demonstrated that alcohols with carbon chain branching at least three carbons away from the -OH group exhibit significantly higher ether selectivity than corresponding alcohols with branches on the α- or β-carbons. Activation energy trends for etherification and dehydration provided a more complete explanation for the ether selectivity trends observed over a range of alcohol structures. Understanding the effects of alcohol structure on direct etherification reactions is crucial for utilizing biomass-derived alcohols to make diesel additives, lubricants, and specialty chemicals.

Experimental Section

Materials

All chemicals obtained commercially were used without further purification. The following chemicals were obtained from Sigma–Aldrich: 1-hexanol (>98%), 1-octanol (>99%), 1-decanol (>99%), 1-dodecanol (>98%), 2-hexanol (>99%), 2-methyl-1-pentanol (>99%), 3-methyl-1-pentanol (>99%), 4-methyl-1-pentanol (>97%), 2-ethyl-1-hexanol (>99%), 2-butyl-1-octanol (>95%), 2-hexyl-1-decanol (>97%), 2-octyl-1-dodecanol (>97%), 2-decyl-1-tetradecanol (97%), dodecane (>99%), hexane (>99%), 1-hexene (>99%), and pyridine (99.8%). The following chemicals were obtained from Spectrum Chemical: 1-heptanol (>98%), 1-octene (>99%), and *n*-tetradecane (>99%), which was used as an internal standard for analytical purposes. The following chemicals were obtained from TCI: 1-nonanol (>99%), 1-undecanol (>99%), di-*n*-octyl ether (>95%), di-*n*-decyl ether (>95%), di-dodecyl ether (>95%), 1-decene (>95%), and 1-dodecene (>95%). Di-*n*-hexyl ether (>98%) was obtained from Alpha Aesar. Synthesis and characterization of 4-hexyl-1-dodecanol is provided in the Supporting Information, Scheme S1, Figures S4–S7.

Synthesis and characterization of tungstated zirconia

Tungstated zirconia (WO_x/ZrO_2, 12.6 wt% W) was synthesized and characterized by using previously reported methods.[19,30,39,40] Powder X-ray diffraction (XRD) patterns for WO_x/ZrO_2 were taken with a Bruker D8 GADDS diffractometer equipped with a CuK_α source (40 kV, 40 mA). Raman spectra were obtained with a LabRAM HR Horiba Scientific Raman spectrometer equipped with a 633 nm^{-1} laser. Brunauer–Emmett–Teller (BET) surface area measurements were performed with a Micrometrics TriStar BET and pretreated with a Micrometrics FlowPrep 060. The ratio of Brønsted- to Lewis-acid sites was determined from IR spectra of adsorbed pyridine, by using a previously reported method.[19] Spectra were acquired with a Thermo Scientific Nicolet 6700 Fourier Transform Infrared Spectrometer (FTIR) equipped with a diffuse reflectance infrared Fourier transform spectrometer (DRIFTS) cell. Inductively coupled plasma (ICP) elemental analysis was performed by Galbraith Laboratories, Inc. to determine tungsten weight loadings.

Batch reactions

All reactions were carried out in sealed 12 mL Q-Tube batch reaction vessels with magnetic stirring at 600 RPM by using an IKA C-MAG HS 10 digital hot plate with temperature control accurate to within ±1 K. A separate batch reaction was performed for each time point for kinetic studies to ensure consistency of volume and concentration of each sample. All reactions over tungstated zirconia were carried out solvent-free with 100 mg of catalyst, 100 μL of *n*-tetradecane as an internal standard, and between 84–205 μL of reactant depending on the reaction conditions (unless otherwise noted). Reaction products were dissolved in acetone for analysis with GC/MS.

Product analysis

The analysis of products was carried out by using a Varian CP-3800 Gas Chromatograph/Mass Spectrometer (GC/MS). The products were quantified with a flame ionization detector (FID) and were identified with a Varian 320 triple quadrupole mass spectrometer (MS). *n*-Tetradecane was used as an internal standard to ensure accurate product quantification. FID response factors for pure commercial compounds were obtained from linear calibration curves, and the effective carbon number method was used to predict response factors for products that are not available in high purity. This method predicts the FID response to within ±1.7%.[41] Mass balances for all reactions were achieved within ±5% unless otherwise noted.

Kinetic analysis

To measure the initial rates of etherification and unimolecular dehydration of 1-hexanol, 1-heptanol, 1-octanol, 1-nonanol, 1-decanol, 1-undecanol, 1-dodecanol, 4-methyl-1-pentanol, 3-methyl-1-pentanol, 2-methyl-1-pentanol, 2-hexanol, and 2-methyl-2-pentanol, individual batch reactions for each time point were carried out at each temperature. Mass transfer limitations were found to be negligible at stirring speeds of 600 RPM for catalyst particle sizes less than 250 μm in diameter. This conclusion was determined by measuring the initial catalytic activity as a function of stirring speed and particle size.

For each experiment, conversion (X_a), selectivity to ether (S_{ether}), selectivity to alkenes ($S_{alkenes}$) were defined as follows:

$$X_a = \frac{\text{moles of a reacted}}{\text{initial moles of a}} \quad (1)$$

$$S_{ether} = \frac{\text{moles of a reacted to form ether}}{\text{moles of a reacted}} \quad (2)$$

$$S_{alkenes} = \frac{\text{moles of a reacted to form alkene}}{\text{moles of a reacted}} \quad (3)$$

Initial rates of ether and alkene formation (r_o) were calculated from the experimentally measured curve of moles of product formed per mass of catalyst versus time (t).

Apparent activation energies were calculated from an Arrhenius plot of the natural log of the initial rates versus the inverse temperature. At low conversions (<25%), the reaction is pseudo-zeroth order in reactant, indicating that the surface of the catalyst is saturated with reactant. Under these conditions, the inhibiting effects of water and ether, and the formation of additional products such as branched ether and oligomerized alkenes are negligible.[19]

The Arrhenius relation was given by:

$$r_o = k_{app} = A_{app}\exp\left(\frac{E_{a,app}}{RT}\right)$$

Where r_o is the initial rate of ether or alkene formation, k_{app} is the apparent rate constant for the reaction, A_{app} is the apparent pre-exponential factor, and $E_{a,app}$ is the apparent activation energy. For the Arrhenius fitting, the pre-exponential factor was fixed for both the etherification and dehydration plots of the C_6 alcohols and linear alcohols, based upon the assumptions that the active sites for each reaction are equivalent, and that the entropy of adsorption of the most abundant surface intermediates and the change in entropy of the transition states are both consistent across the various substrates. The pre-exponential factors were fit to minimize the standard error on the least squares regression for each group of substrates. Error bars for activation energies were taken from the standard error of the least squares regression. Arrhenius plots, initial rates, pre-exponential factors, activation energies, and the temperature ranges for each reaction are given in Figures S2–S3 and Tables S1–S4 in the Supporting Information.

Acknowledgements

This work was initiated with funding from the Energy Biosciences Institute and completed with funding from the Director, Office of Science, Office of Basic Energy Sciences of the U.S. Department of Energy under Contract No. DE-AC02-05CH11231. J. Rorrer would also like to acknowledge funding from the National Science Foundation Graduate Research Fellowship (Grant Number DGE 1106400). The authors thank Adam Grippo, Deepak Jadhav, Amit Gokhale, Christopher Ho, and Konstantinos Goulas for useful discussions.

Conflict of interest

The authors declare no conflict of interest.

Keywords: alcohol coupling · biomass derivation · diesel additives · etherification · tungstated zirconia

[1] C. Sievers, Y. Noda, L. Qi, E. M. Albuquerque, R. M. Rioux, S. L. Scott, *ACS Catal.* **2016**, *6*, 8286 – 8307.
[2] R. J. J. Nel, A. De Klerk, *Ind. Eng. Chem. Res.* **2009**, *48*, 5230 – 5238.
[3] A. Arteconi, A. Mazzarini, G. Di Nicola, *Water Air Soil Pollut.* **2011**, *221*, 405 – 423.
[4] A. L. Maximov, A. I. Nekhaev, D. N. Ramazanov, *Pet. Chem.* **2015**, *55*, 1 – 21.
[5] J. Guilera, E. Ramírez, C. Fité, J. Tejero, F. Cunill, *Catal. Sci. Technol.* **2015**, *5*, 2238 – 2250.
[6] M. J. Pilling, *Low-Temperature Combustion and Autoignition*, Elsevier, Amsterdam, **1997**.
[7] D. A. Law, L. R. Rudnick, R. A. Kremer, Patent US 5552071 A, **1996**.
[8] W. Beilfuss, R. Gradtke, W. Siegert, K.-H. Diehl, K. Weber, US 7268102 B2, **2007**.
[9] D. Jadhav, A. M. Grippo, S. Shylesh, A. A. Gokhale, J. Redshaw, A. T. Bell, *ChemSusChem* **2017**, *10*, 2527 – 2533.
[10] T. Zolper, Z. Li, C. Chen, M. Jungk, T. Marks, Y.-W. Chung, Q. Wang, *Tribol. Lett.* **2012**, *48*, 355 – 365.
[11] R. Benda, J. Bullen, A. Plomer, *J. Synth. Lubr.* **1996**, *13*, 41 – 57.
[12] N. Qureshi, H. P. Blaschek, *J. Ind. Microbiol. Biotechnol.* **2001**, *27*, 287 – 291.
[13] T. J. Schwartz, B. J. O'Neill, B. H. Shanks, J. A. Dumesic, *ACS Catal.* **2014**, *4*, 2060 – 2069.
[14] S. Sreekumar, Z. C. Baer, E. Gross, S. Padmanaban, K. Goulas, G. Gunbas, S. Alayoglu, H. W. Blanch, D. S. Clark, F. D. Toste, *ChemSusChem* **2014**, *7*, 2445 – 2448.
[15] P. Anbarasan, Z. C. Baer, S. Sreekumar, E. Gross, J. B. Binder, H. W. Blanch, D. S. Clark, F. D. Toste, *Nature* **2012**, *491*, 235 – 239.
[16] C. Carlini, A. Macinai, A. M. Raspolli Galletti, G. Sbrana, *J. Mol. Catal. A* **2004**, *212*, 65 – 70.
[17] M. Balakrishnan, E. R. Sacia, A. T. Bell, *Green Chem.* **2012**, *14*, 1626 – 1634.
[18] R. C. C. Pereira, V. M. D. Pasa, *Fuel* **2006**, *85*, 1860 – 1865.
[19] J. Rorrer, Y. He, F. D. Toste, A. T. Bell, *J. Catal.* **2017**, *354*, 13 – 23.
[20] S. Roy, G. Mpourmpakis, D. Hong, D. G. Vlachos, A. Bhan, R. J. Gorte, *ACS Catal.* **2012**, *2*, 1846 – 1853.
[21] P. Kostestkyy, J. Yu, R. J. Gorte, G. Mpourmpakis, *Catal. Sci. Technol.* **2014**, *4*, 3861 – 3869.
[22] G. Larsen, E. Lotero, L. M. Petkovic, D. S. Shobe, *J. Catal.* **1997**, *169*, 67 – 75.
[23] M. Kang, J. F. DeWilde, A. Bhan, *ACS Catal.* **2015**, *5*, 602 – 612.
[24] R. Bringué, E. Ramírez, M. Iborra, J. Tejero, F. Cunill, *Chem. Eng. J.* **2014**, *246*, 71 – 78.
[25] C. Casas, R. Bringué, E. Ramírez, M. Iborra, J. Tejero, *Appl. Catal. A* **2011**, *396*, 129 – 139.
[26] E. Medina, R. Bringué, J. Tejero, M. Iborra, C. Fité, *Appl. Catal. A* **2010**, *374*, 41 – 47.
[27] I. Hoek, T. A. Nijhuis, A. I. Stankiewicz, J. A. Moulijn, *Appl. Catal. A* **2004**, *266*, 109 – 116.
[28] J. Guilera, R. Bringué, E. Ramírez, M. Iborra, J. Tejero, *Ind. Eng. Chem. Res.* **2012**, *51*, 16525 – 16530.
[29] J. A. Melero, J. Iglesias, G. Morales, *Green Chem.* **2009**, *11*, 1285 – 1308.
[30] Y. Zhao, W. Li, M. Zhang, K. Tao, *Catal. Commun.* **2002**, *3*, 239 – 245.
[31] S. R. Ginjupalli, S. Mugawar, N. P. Rajan, P. Kumar Balla, V. R. C. Komandur, *Appl. Surf. Sci.* **2014**, *309*, 153 – 159.
[32] G. Larsen, E. Lotero, S. Raghavan, R. D. Parra, C. A. Querini, *Appl. Catal. A* **1996**, *139*, 201 – 211.
[33] R. Balzer, V. Drago, W. H. Schreiner, L. F. D. Probst, *J. Braz. Chem. Soc.* **2014**, *25*, 2026 – 2031.
[34] S. Kuba, P. Concepción Heydorn, R. K. Grasselli, B. C. Gates, M. Che, H. Knözinger, *Phys. Chem. Chem. Phys.* **2001**, *3*, 146 – 154.
[35] D. E. López, K. Suwannakarn, D. A. Bruce, J. G. Goodwin, *J. Catal.* **2007**, *247*, 43 – 50.
[36] E. R. Sacia, M. Balakrishnan, M. H. Deaner, K. A. Goulas, F. D. Toste, A. T. Bell, *ChemSusChem* **2015**, *8*, 1726 – 1736.
[37] H. Pines, W. O. Haag, *J. Am. Chem. Soc.* **1961**, *83*, 2847 – 2852.
[38] M. Balakrishnan, E. R. Sacia, A. T. Bell, *ChemSusChem* **2014**, *7*, 1078 – 1085.
[39] C. D. Baertsch, S. L. Soled, E. Iglesia, *J. Phys. Chem. B* **2001**, *105*, 1320 – 1330.
[40] M. Hino, K. Arata, *J. Chem. Soc. Chem. Commun.* **1988**, 1259 – 1260.
[41] R. D. Down, J. H. Lehr, *Environmental Instrumentation and Analysis Handbook*, Wiley, Hoboken, **2005**.

Manuscript received: May 15, 2018
Revised manuscript received: June 15, 2018
Accepted manuscript online: July 25, 2018
Version of record online: August 23, 2018